



FEA Modelling of Externally-Strengthened Concrete Beam with CFRP Plates Under Flexural Test

Malik Ridwan Maulana¹, Hilton Ahmad^{1*}, Hazrina Mansor²

¹Faculty of Civil Engineering and Built Environment,
Universiti Tun Hussein Onn Malaysia, 86400 Parit Raja, Johor, MALAYSIA

²School of Civil Engineering,
Universiti Teknologi MARA, 40450 Shah Alam, Selangor, MALAYSIA

*Corresponding Author

DOI: <https://doi.org/10.30880/ijie.2022.14.05.029>

Received 26 June 2022; Accepted 15 August 2022; Available online 25 August 2022

Abstract: This study concentrates on FEA modelling of concrete beam strengthened with externally bonded CFRP plates under bending by using Traction Separation Law (TSL) as constitutive law to require maximum cohesive stress and fracture energy values. The FEA models were developed following experimental work reported by Al-Rousan et al. [23] and Ding et al. [22]. Combination of two numerical techniques were adopted, i.e., Extended Finite Element Method (XFEM) and Cohesive Zone Method (CZM) assigned within cracked beam region and adhesive layer respectively. The consistence of FEA beam deformations to capture debonding failure as seen during experimental observations and load-displacement was evaluated accordingly. Additionally, combination of XFEM-CZM techniques provides good strength predictions with experimental dataset. It is clearly shown that the failure mode exhibited are determined by testing method, CFRP width and CFRP length. CFRP sheets provides a significant contribution to concrete ductility, which is noticeable in longest CFRP sheet. All testing series were examined, the discrepancies of less than 25% were found. Note that current approach used calibrated fracture energy values from similar concrete grade and CFRP plates, however better prediction can be produced if fracture energy values were independently determined from experimental set-up.

Keywords: Beam strengthening, TSL, XFEM, CZM, delamination, shear failure, CFRP

1. Introduction

Application of composite materials to repair and strengthen concrete structures has been considered as an effective, convenient and practical solution. Fiber reinforced polymer (FRP) composite system are adopted due to excellent mechanical properties, fatigue resistance, manufacturing flexibility and available in variety forms [1]. Numerous studies were reported to strengthening techniques of concrete beam such as externally-bonded [2], near surface mounted [3], composite fiber reinforced polymer [4] and etc. Regards to externally-bonded, three schemes types were most commonly used such as bottom side [5], side-bonded [6] and U-wrap [7]. Three prominent failure modes were observed. i.e., FRP rupture, shear failure and debonding dependent upon several factors such as FRP length, beam size and presence of notch. Additionally, NCHRP-549 [8] classified two shear failure types consists of web-shear crack and flexure-shear crack as beam loaded under four-points bending. Similar findings were seen in three-points bending with stiff and strong FRP system to resist the initial flexural crack but eventually exhibited shear failure mode [9]. Nevertheless, according to FIB [10] the failure prone to occur between concrete beam and externally-bonded FRPs with presence of slip to exhibit cohesive failures of localized delamination.

Carbon fiber reinforced polymer (CFRP) is the most widely used FRP types in external strengthening work due to high elastic modulus, superior strength and excellent elongation at break. Ali et al. [11] investigated reinforced concrete beam strengthened with CFRP and GFRP and found that strengthening by CFRP is favorable compared to GFRP sheet. Moreover, Mostofinejad & Moghaddas [12] investigated reinforced concrete beam with two strengthening approaches by conventional externally-bonded reinforcement and externally bonded reinforcement on grooves. It found that former approach improves the load capacity to 27% while latter approach increased to 39%. More recently, De Domenico et al. [13] tested two different systems of notched concrete beam of CFRP strengthening and fiber reinforced cementitious matrix (FRCM) with poly-benzoxole (PBO) grid on under different elevated temperatures. It was found that CFRP strengthened beam at 50°C curing condition showed 30% peak load reduction as compared to control specimens. Nevertheless, all strengthened concrete beam specimens with CFRP exhibited debonding failure modes which is more progressive and favorable among structures engineers in externally-bonded strengthening.

Traditional FEA modelling simulated crack propagations and requires very fine mesh ahead of the crack tip due to the presence of stress singularity. Traction-separation relationship is derived from state-of-the-art fracture mechanics fundamental can be incorporated as constitutive model within FEA modelling framework to require only maximum cohesive stress, σ_0 (here refers as unnotched concrete strength) and fracture energy value, G_c . Hence, this material model is driven by energetic approach to eliminate the requirement of mesh refinement ahead of the crack tip. Available modelling techniques can be adopted such as are extended finite element method (XFEM), cohesive zone model (CZM) and virtual crack closure technique (VCCT) embedded within ABAQUS CAE 2021. Yee & Ahmad [14] developed FEA models by implementing XFEM frameworks of single lap kenaf fiber composite hybrid joint under quasi-static loading. The result demonstrated good agreement between experimental datasets and FEA modelling with discrepancy of less than 5%. Subsequently, Nunes et al. [15] incorporates CZM technique under mixed modes failure based on experimental observations and chosen mixed-mode criteria for adhesives was successfully validated. Additionally, Orifici & Krueger [16] conducted benchmarking works by implementing VCCT on end-notched flexure specimen. It was found that VCCT able to replicate delamination growth under static loading. The study conducted by [17] applied combination techniques of XFEM-CZM and XFEM-VCCT to simulate double cantilever composite beam (DCB) of delamination propagation under quasi-static loading and found that CZM-XFEM method is the most applicable delamination modelling technique. Tafazzolmoghaddam [18] expands fatigue delamination modelling using XFEM-CZM under high cycle loading and revealed that CZM-based fatigue model does not predict uniform degradation rate along CZM failure path.

This paper aims to provide FEA benchmarking work of experimental programme reported in Al-Rousan et al. [23] and Ding et al. [22] of unnotched and notched beam externally-strengthened with CFRP plates respectively. Two prominent failure modes were reported, i.e., shear failure and delamination and the models are developed following the failure mode exhibited using ABAQUS CAE 2021. A physically-based traction-separation law (TSL) relationship by incorporating combined XFEM-CZM is used for delamination failure. Additionally, shear failure mode only adopted XFEM within cracked regions as no FRP fracture was seen experimentally.

2.1 Traction Separation Law as Constitutive Model

The traction-separation law (TSL) was proposed by Camanho et al. [19] within ABAQUS CAE to investigate fracture and failure behavior of materials under mixed-mode criterion. TSL defines the functional form of applied traction in dependence on separation distance. As an element are separates, a quantity of energy equal to the critical fracture energy of material is released. The constitutive model of TSL describes displacement jump (δ) and traction (T) as an interface to simulate crack nucleation, initiation and propagation. The cohesive element recovers linear behavior to a triangular law employed within FEA software until the tensile separation reached maximum traction opening once damage has taken place within respective failed cohesive element as given in Fig. 1(a). In mixed-mode failure criterion (Fig.1(b)), cohesive separation is dominated by the displacement jump normal to interface as Mode I dominated but cohesive separation is controlled by shear displacement in the Mode II dominated applies. Regards to separation mode, TSL requires three parameters, i.e., initial stiffness, K_n , maximum traction, σ_0 and fracture energy, G_c [17]. Two modelling techniques, i.e., extended finite element method (XFEM), cohesive zone model (CZM) can be adopted in conjunction of TSL model and described in the following sections.

2.2 Extended Finite Element Method (XFEM)

In order to model stationary discontinuities like a crack with conventional FEM, the mesh must adhere to the geometric discontinuities. Therefore, to fully capture to singular asymptotic fields, extensive mesh refinement is required at the vicinity of the crack tip. It is significantly challenging to model a developing fracture as the mesh has to be updated constantly to fit the discontinuity geometry as the crack propagated. The theoretical underpinning XFEM is to address discontinuous issues like fractures by introducing the local enrichment function into the element displacement term of conventional FEM. The equation of displacement function (u) around the crack tip is expressed in Eq. (1). The study conducted by Karimi & Rouzegar [20] describes four functions of elastic solution to assume as a function of asymptotic crack tip using polar local coordinate as given in Eq. (2). Additionally, the discontinuity of displacement for failed nodes associated to crack can be enriched by using Heaviside function in Eq. (3).

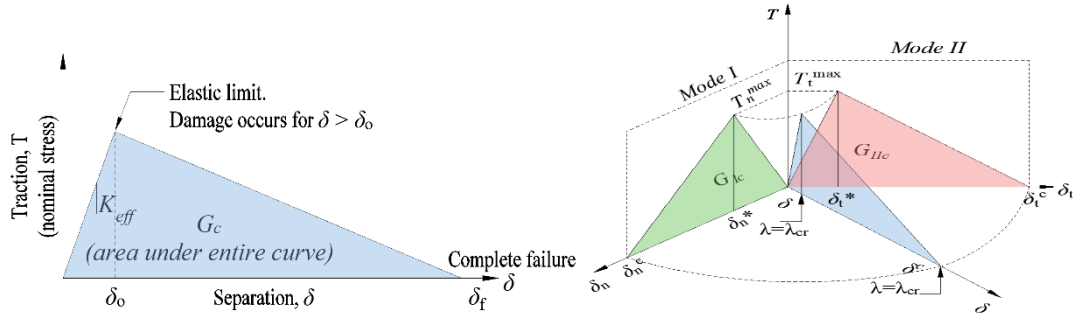


Fig. 1 - Traction separation law in (a) principal mode (b) mixed-modes.

$$u = \sum_{I=1}^N N_I(x) \left[u_I + H(x) a_I + \sum_{a=1}^4 F_a(x) b_I^a \right] \tag{1}$$

where $N_i(x)$ is node i shape function matrix, N is element node number, u_I is the finite element displacement vector, $H(x)$ is Heaviside function to represent discontinues jump, F_a is an asymptotic crack tip function, a value is varied from 1-4, and b_I are standard Node i degree of freedom.

$$F_a(r, \theta) = \left\{ \sqrt{r} \sin\left(\frac{\theta}{2}\right), \sqrt{r} \cos\left(\frac{\theta}{2}\right), \sqrt{r} \sin\left(\frac{\theta}{2}\right) \sin(\theta), \sqrt{r} \cos\left(\frac{\theta}{2}\right) \sin(\theta) \right\} \tag{2}$$

$$H_{(x)} = \begin{cases} 1 \text{ for } (x - x^*) \cdot e_n > 0 \\ -1 \text{ for } (x - x^*) \cdot e_n < 0 \end{cases} \tag{3}$$

where e_n describe as unit normal vector, x is Gaussian integral vector displacement, x^* is the nearest displacement vector from x on the crack boundary.

As can be seen from Fig. 2, related finite element mesh of 2D crack body consisting of crack line as dash line. Additionally, finite element mesh is represented by solid line and node is depicted as black circular dot. The first crack within XFEM is surrounded by two nodes of the rectangular blue shape named Heaviside enrichment node (set J). Another node type is crack tip node (set K) and represented as red circular node. The XFEM formulation concept is similar with conventional FEM based on Galerkin’s formulation.

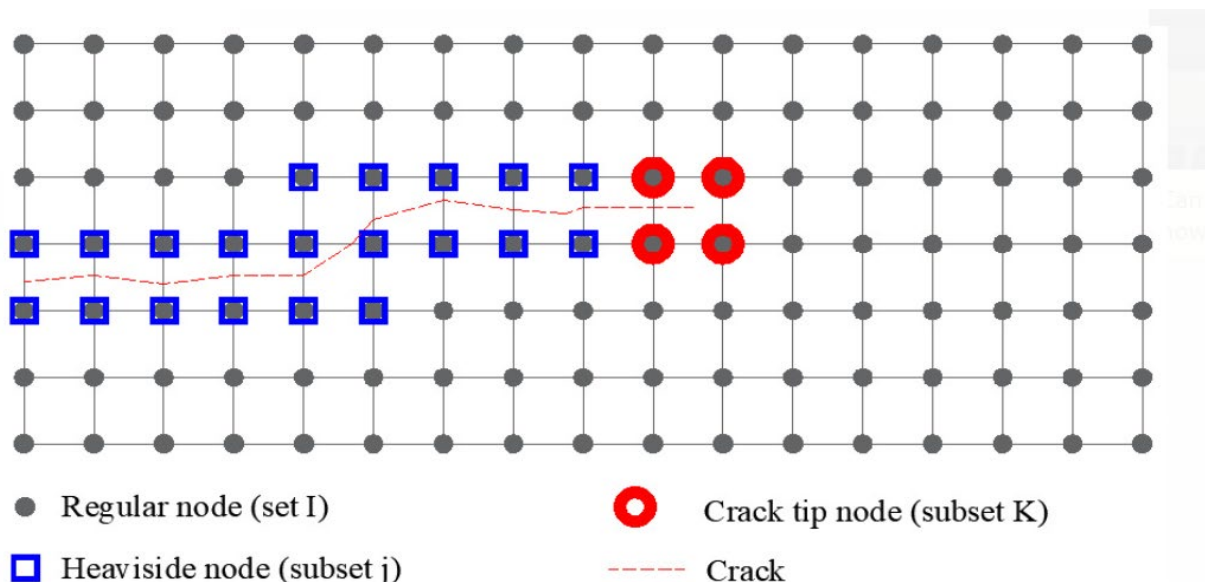


Fig. 2 - Two-dimensional finite element mesh

2.3 Cohesive Zone Model (CZM)

The cohesive zone model (CZM) is a fracture mechanic model in which crack formation is viewed as a progressive process and crack surface separation occurs across a prolonged crack tip or cohesive zone which is resisted by cohesive traction. According to Rarani & Sayedain [17] description of cohesive stress from applied traction is given in Fig. 3, followed by linear softening upon fracture initiation and expressed as scalar damage variable, D and later increased monotonically as damage occurs. If damage values are specified, then stress values are reduced accordingly. The linear traction-separation behavior intersection occurs with slope of $(1-D)K_n$. The softening response of cohesive element are represented by using normal and shear components from elastic traction-separation as given in Eq. (4).

$$t_{(n)} = \begin{cases} (1-D) \cdot t_n^0, & t_n^0 \geq 0 \\ t_n^0, & t_n^0 \leq 0 \end{cases}, \quad t_{(s)} = (1-D) \cdot t_s^0, \quad t_{(t)} = (1-D) \cdot t_t^0 \quad (4)$$

CZM is widely reported to simulate delamination in composite materials where it is prominently induced by cracking within laminates matrix. Thus, the cohesive strength represented as maximum matrix stress, σ_0 within cohesive layer to reach matrix strength. The crack appears once adhesion force (to represent applied traction) has reached maximum matrix stress, followed by crack propagations due to extended two separated faces. The body structure is still intact state in low loading condition and progressively increased as cohesive element is failed gradually. The function response between two separated interface is calculated based on crack initiation criterion and tabulated in Table 1 extracted from Zhang et al. [21].

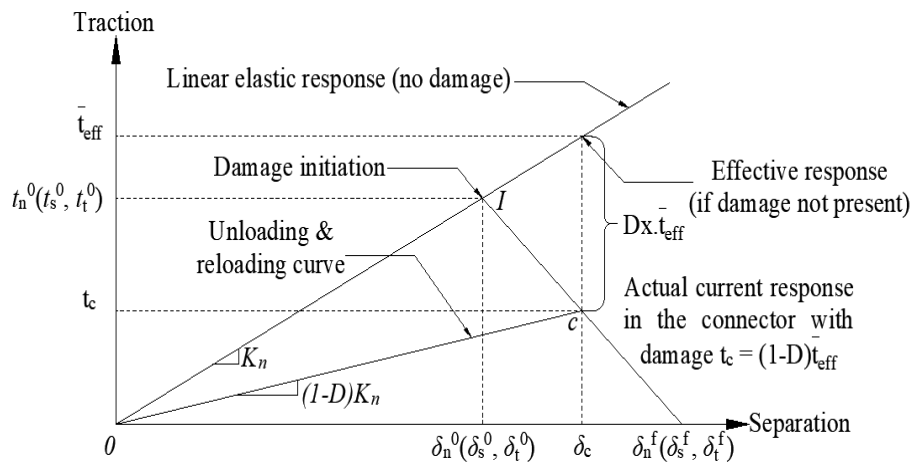


Fig. 3 - Bilinear traction separation response of CZM

Table 1 - Damage initiation criterion of CZM

Criterion	Criterion Law
Maximum principal stress criterion (MAXPS)	$f = \left\{ \frac{\langle \sigma_{max} \rangle}{\sigma_{max}^0} \right\}$
Maximum principal strain criterion (MAXPE)	$f = \left\{ \frac{\langle \epsilon_{max} \rangle}{\epsilon_{max}^0} \right\}$
Maximum nominal stress criterion (MAXS)	$f = \left\{ \frac{\langle t_n \rangle}{t_n^0}, \frac{t_s}{t_s^0}, \frac{t_t}{t_t^0} \right\} = 1$
Maximum nominal strain criterion (MAXE)	$f = \left\{ \frac{\langle \epsilon_n \rangle}{\epsilon_n^0}, \frac{\epsilon_s}{\epsilon_s^0}, \frac{\epsilon_t}{\epsilon_t^0} \right\} = 1$
Quadratic traction interaction criterion (QUADS)	$f = \left\{ \frac{\langle t_n \rangle}{t_n^0} \right\}^2 + \left\{ \frac{t_s}{t_s^0} \right\}^2 + \left\{ \frac{t_t}{t_t^0} \right\}^2 = 1$
Quadratic separation interaction criterion (QUADE)	$f = \left\{ \frac{\langle \epsilon_n \rangle}{\epsilon_n^0} \right\}^2 + \left\{ \frac{\epsilon_s}{\epsilon_s^0} \right\}^2 + \left\{ \frac{\epsilon_t}{\epsilon_t^0} \right\}^2 = 1$

3. Finite Element Modelling

ABAQUS CAE 2021 allows modelling of fracture and failure of structures body without the requirement for remeshing. XFEM technique is used to analyze fracture initiation and propagation along arbitrary solution dependent path. Here, combination of CZM and XFEM techniques is used to predict the 2D crack propagation Nevertheless, FEA models using constitutive model requires few material properties datasets and if possible, these values are calibrated prior to FEA analysis [16].

3.1 Testing Series Investigated

Benchmarking works were carried out following two experimental programme reported by Ding et al. [22] and Al-Rousan et al. [23] tested under three-points bending of initial crack of notched concrete beam and four points bending of un-notched beam, both studies are strengthened with CFRP sheet. Testing series of both works has various CFRP length bonded on tension concrete beam face as given in Table 2. Ding et al. [22] introduced sharp notch at the mid-span of concrete specimen with a constant notch height, a_0 of 20 mm and notch opening width a_1 of 3 mm with beam size of $500 \times 100 \times 100 \text{ mm}^3$. On the contrary, Al-Rousan et al. [23] conducted un-notched concrete beam of similar beam size. Fig. 4 and Fig. 5 showed detail schematic testing specimen used in Ding et al. [22] and Al-Rousan et al. [23], respectively. The CFRP thickness used in both Ding et al. [22] and Al-Rousan et al. [23] is specified as 0.111 mm and 0.166 mm, respectively which is externally bonded using epoxy resin.

Table 2 - Testing designations as a function of CFRP sizes used in both benchmarking studies

Ding et al. [22]			Al-Rousan et al. [23]		
Designation	CFRP length (mm)	CFRP width (mm)	Designation	CFRP length (mm)	CFRP width (mm)
20-000	No CFRP (control)	-	G1-F0-0-N	No CFRP (control)	-
20-100	100	100	G1-F0-10-N	100	50
20-150	150	100	G1-F0-15-N	150	50
20-200	200	100	G1-F0-20-N	200	50
20-300	300	100	G1-F0-25-N	250	50
20-350	350	100			

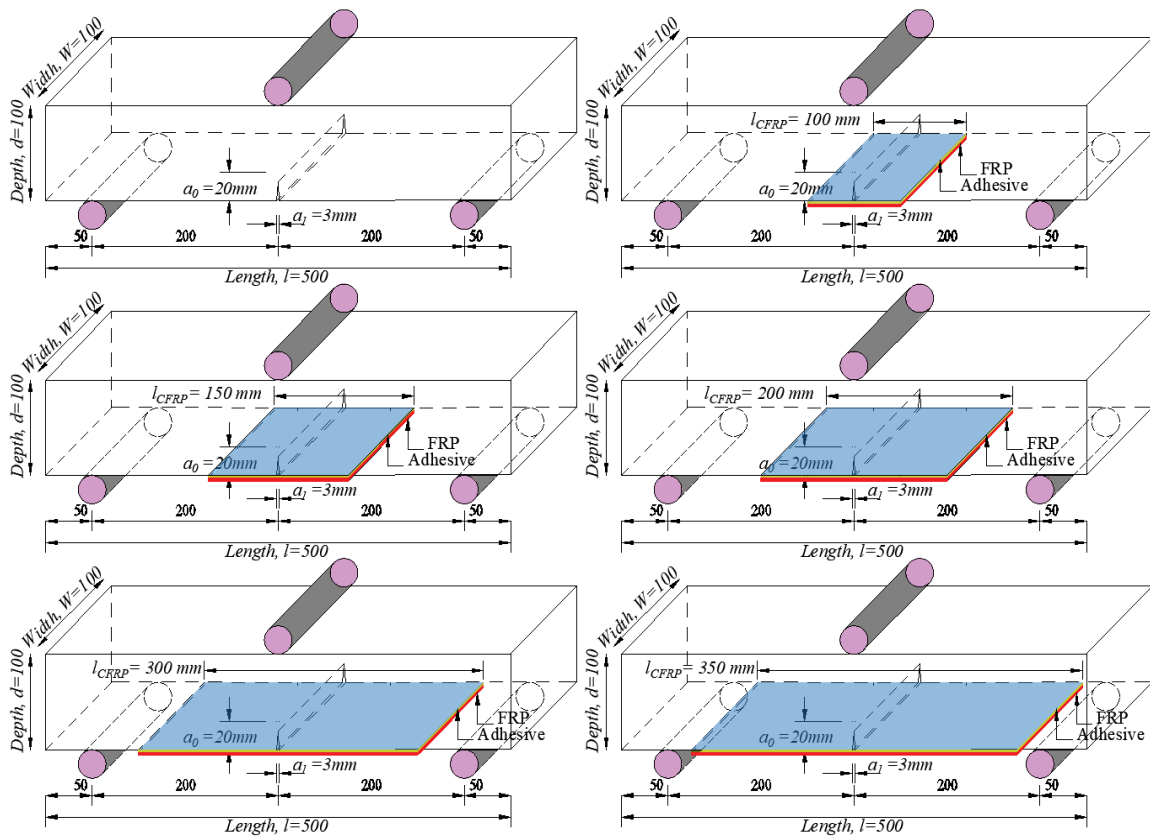


Fig. 4 - Detail schematic test for Ding et al. [22] (all units in mm)

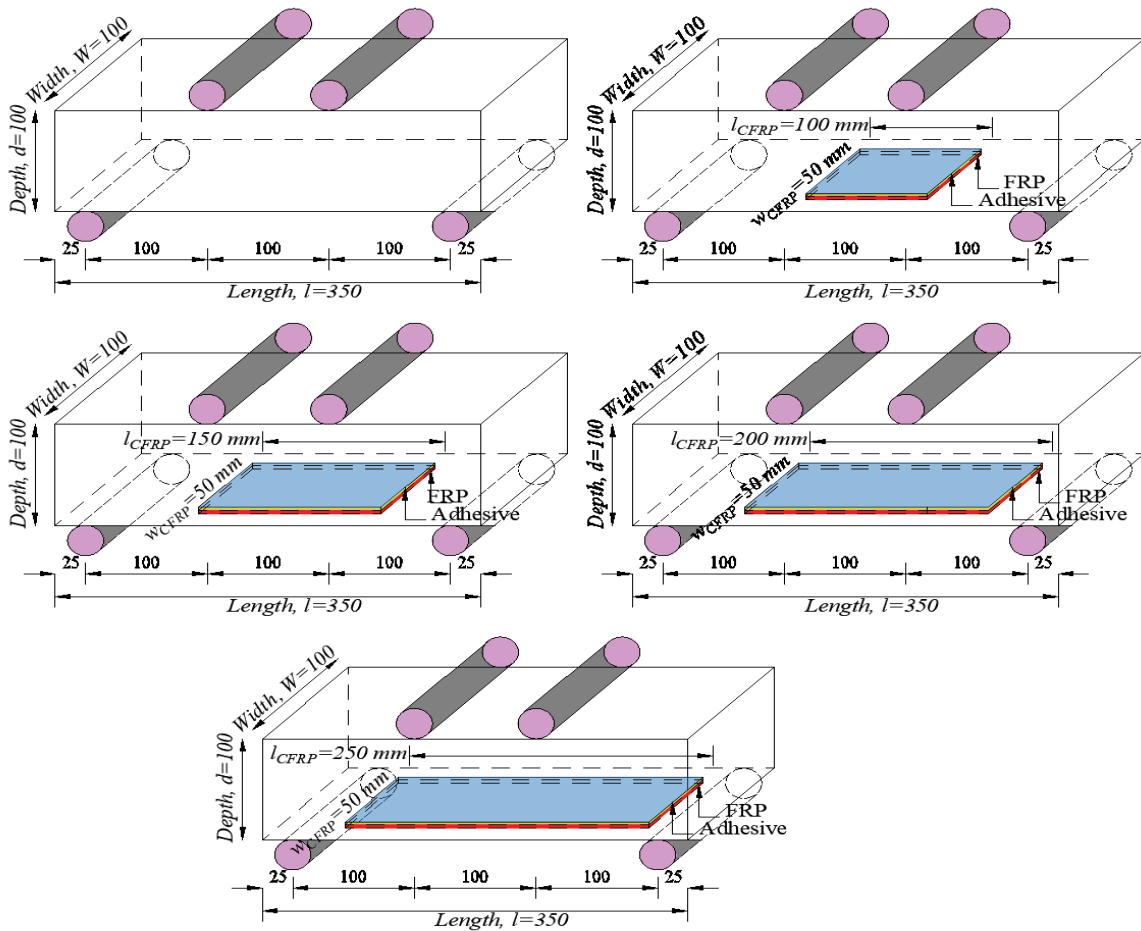


Fig. 5 - Detail schematic test for Al-Rousan et al. [23] (all units in mm)

3.2 Material Properties

As previously mentioned, the FEA Modelling were developed using combination of XFEM and CZM techniques to incorporate TSL model and requires material properties datasets. Nevertheless, material properties both for Ding et al. [22] (notched) and Al-Rousan et al. [23] (unnotched) were calibrated from other studies which tabulated in Table 3. The material properties were given from (after Ding et al. [22], Mahmoud [24], Mohammadi & Wan [25], Darwin et al. [26], Al-Rousan et al. [23], Rodrigues et al. [27], Mahjoub et al. [28], Kasper et al. [29], and Wang & Wu [30]).

Table 3 - Material properties required in FEA Modelling

Material properties		CFRP sheet		Adhesive		Concrete	
		Unnotched	Notched	Unnotched	Notched	Unnotched	Notched
Young's modulus, E (GPa)	E_x	165 ^a	230 ^c	3.18 ^c	9.6 ^a	32.89 ^a	33.10 ^c
	E_y	17.9 ^b					
	E_z	17.9 ^b					
Poisson's ratio, ν	ν_{xy}	0.22 ^a					
	ν_{yz}	0.22 ^a		0.34 ^c	0.30 ^a	0.28 ^a	
	ν_{xz}	0.30 ^b					
Shear modulus, G (GPa)	G_{xy}	11.79 ^b					
	G_{xz}	11.79 ^b					
	G_{yz}	6.88 ^b					
Unnotched strength, σ_0 (MPa)		3500 ^b		4.5959 ^c	12.94 ^f	5.15 ^a	2.97 ^e
Shear strength, τ_s (MPa)				5.13 ^c	14 ^g		
Fracture energy, G_I (N/mm)	G_{IC}			0.2 ^c	0.41 ^h	0.127 ^d	0.147 ^e
	G_{IIC}			0.366 ^c	1.19 ⁱ		

3.3 Pre-processing Stages

Two-dimensional model of concrete beam strengthened with FRP sheets under flexural conditions were developed, following experimental set-up conducted. All models comprised of five parts, i.e., concrete beam, FRP, adhesive, punch and support. Fig. 6 shown assembled parts to reproduce the concrete beam tested under four-points bending test. Surface contact interaction between punch and supports (as rigid part) and concrete beam surface as master and slave interaction respectively. This model labelled master surface as red color while slave surfaces are given as purple. Assigning proper frictions behavior between master and slave surfaces to allow stress transfer between adjacent parts. The friction coefficient used in this model was set as small value of 0.001 and small sliding was chosen to allow infinitely small node movement.

Sufficient mesh refinements were used in order to prevent from mesh-dependent and performed in sensitivity study work. Constitutive model employed in the current work requires unnotched strength, σ_o and fracture energy, G_c of cracked material within adhesive layer (MAXS damage criterion). Both punches were assigned as a control point by coupling and displacement were applied downward to denote applied load. Additionally, both supports were set as pinned and roller at the left and right supports respectively.

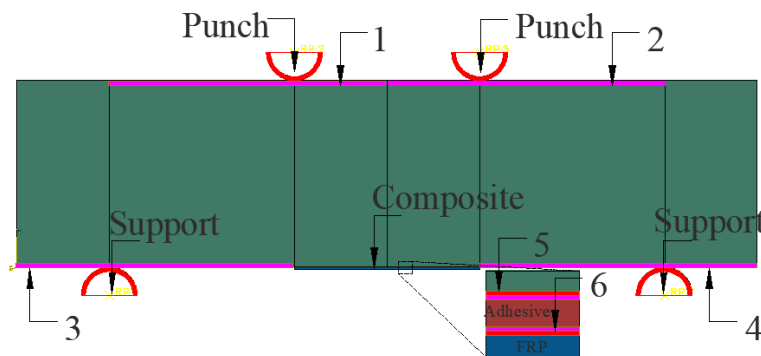


Fig. 6 - Assembling of composite beam in ABAQUS CAE

4. Sensitivity Study

Sensitivity study was performed to assure the strength predictions work is independent of damage stabilization coefficient and mesh refinements, given in the following sub-sections.

4.1 Damage Stabilization Coefficient

Softening in the material model requires damage evolution behavior to demonstrate convergence issues. Viscous regularization is used within ABAQUS CAE to give steady response during damage evolutions. The tangent stiffness matrix is positive in sufficiently small time-steps and viscosity coefficient incorporated MAXPS Damage criterion to ease convergence. This study investigates damage stabilization coefficient increments from 1×10^{-1} to 1×10^{-10} and strength prediction obtained are shown in Fig. 7 for notched concrete beam specimens following Ding et al. [22]. It was found that small damage stabilization coefficient leading to difficulties in convergence solutions. On the other hand, large damage stabilization coefficient leading to excessive and non-physical strength prediction output. Small damage stabilization coefficient is associated to convergence difficulties but usually promotes reliable predictions. As seen in Fig. 7, damage tolerance of 1×10^{-5} was sufficient as it started to show plateau and no difference of strength prediction output as lower values of damage coefficients is used. Similar study is also performed in un-notched beam series from Al-Rousan et al. [23] and not repeated here.

4.2 Mesh Sensitivity

An analytical studies carried out by Munjiza & John [31] states that finite element size was close to the fracture tip requires much smaller size than the plastic zone length to achieve accurate result in 2-D fracture simulation. Meanwhile, also their study also revealed theoretical estimation of the plastic zone length (Δ) which expressed in Eq. (5). Beside mesh size, mesh orientation takes crucial part in mesh sensitivity analysis. The 2-D model used in this study is free-mesh to allow crack propagates through quadrilateral element boundaries. It is emphasized that unstructured meshes might lessen global mesh dependency, but fracture path is still dependent upon local mesh orientation. The study conducted by Tijssens et al. [32] have shown that cohesive zone model shows mesh dependency of fracture pattern in structured meshes, which means the fractures tend to propagate along dominant direction of element alignment.

This study investigates several mesh densities to ensure strength prediction is independent upon mesh refinement. The global mesh size studied are in the range between 10 to 0.5 (indicates coarser to more fine mesh sizes). In the shell-based formulation, within this study is modelled using four-nodded shell elements (ABAQUS designation as CPE4R).

From FEA fundamental, finer mesh yields highly accurate results but may take more computational effort [33]. On the contrary, FE models with larger mesh may leads to less accurate result but faster computational time. Additionally, finer mesh size increase the model stiffness and prone to reduce displacement and stress exhibition [34]. As shown in Table 4 and Table 5, ultimate load at failure were independence of global mesh size as constitutive model incorporated is driven by energetic approach.

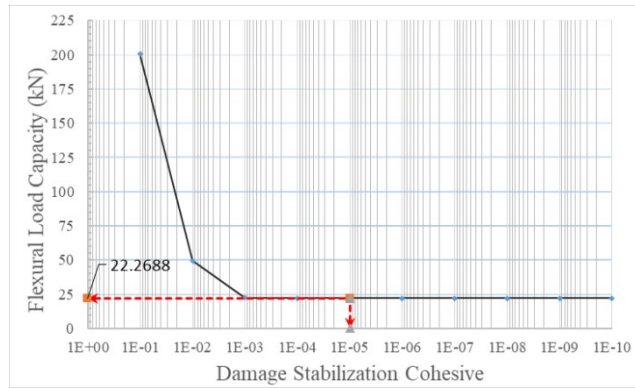


Fig. 7 - Damage stabilization coefficients used for in notched beam (after Ding et al. [22])

$$\Delta_{short} = \frac{E}{4f_t} \delta_c = \frac{3EG_f}{4f_t^2}, \Delta_{long} = \frac{\pi E}{32f_t} \delta_c = \frac{3\pi EG_f}{4f_t^2}, \text{ which is } \Delta_{long} \leq \Delta \leq \Delta_{short} \quad (5)$$

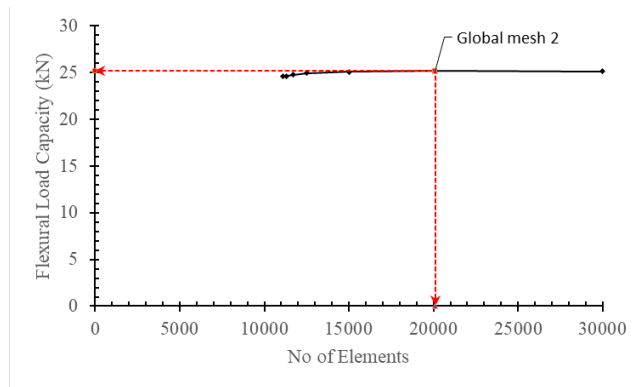


Fig. 8 - Mesh refinement study of unnotched beam (after Al-Rousan et. al [23])

Table 4 - Detail meshing within ABAQUS for notched beam

Part	Global mesh	No of elements	No of nodes	P_{ult} (kN)	δ_{ult} (mm)
Beam	10	2118	2216	22.27	0.42
	8	2598	2708	22.34	0.38
	6	3398	3528	22.73	0.27
	4	5078	5250	22.28	0.21
	2	10118	10416	22.28	0.18
	1	20038	20584	22.84	0.18
CFRP	0.5	39878	40920	22.47	0.18
	0.5	699	1054	-	-

Table 5 - Detail meshing within ABAQUS for unnotched beam

Part	Global mesh	No of elements	No of nodes	P _{ult} (kN)	δ _{ult} (mm)
Beam	10	11100	11312	24.61	0.34
	8	11300	11514	24.63	0.28
	6	11700	11918	24.76	0.22
	4	12500	12726	24.92	0.19
	2	15000	15251	25.08	0.18
	1	20100	20402	25.17	0.18
CFRP	0.5	30000	30401	25.14	0.18
	0.5	600	804	-	-

5. Results and Discussion

This section describes post-processing outputs and the comparison with the experimental dataset. From respective experimental observation, all unnotched beam specimens (from Al-Rousan et.al. [23]) showed delamination failures in all CFRP length series. On the contrary, in notched beam series demonstrates two prominent failure modes (i.e., delamination and shear failure) dependence upon CFRP length. All tested beam designations were modelled according to failure mode reported. These finding are presented in the following section by describing damage plot, FEA consistency with experimental observations and validation to experimental datasets.

5.1 Damage Plot under Delamination Mode

A typical load-displacement profile from initial loading until fully failed of concrete specimen failed delamination mode is represented by model designation of 20-350 for notched beam as depicted in Fig 9. Associated damage plot of labelled key-points is given subsequently in Fig. 10. As load from punch is applied, the stress is gradually increased linearly until it reached point A. Here, the cracked concrete beam has propagated until certain length and simultaneously, CFRP plates also experience applied stress due to bending. Prior to point B adhesive have not yet deformed but promotes to cracked beam propagation. As it reached point B, adhesive has started to lose its loading capacity by showing element deletion within cohesive element from mid-spa and propagates to CFRP edge. Point C is showing the CFRP ductility for beam strengthening until sudden failure as labeled at point D.

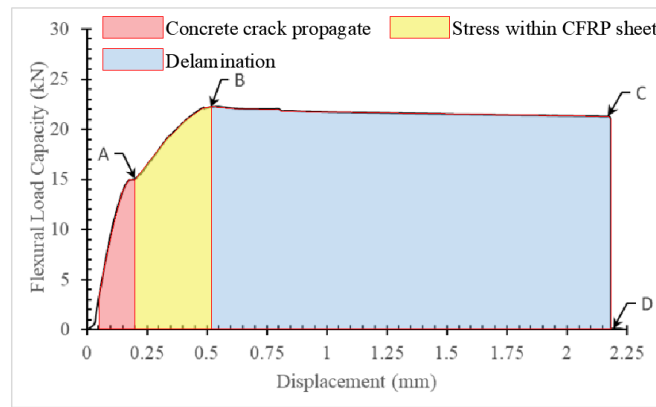
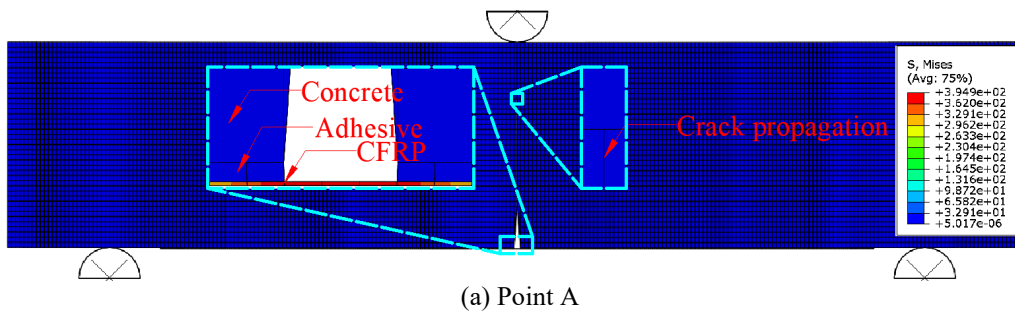


Fig. 9 - Load-displacement profile of concrete beam specimens failed in delamination mode



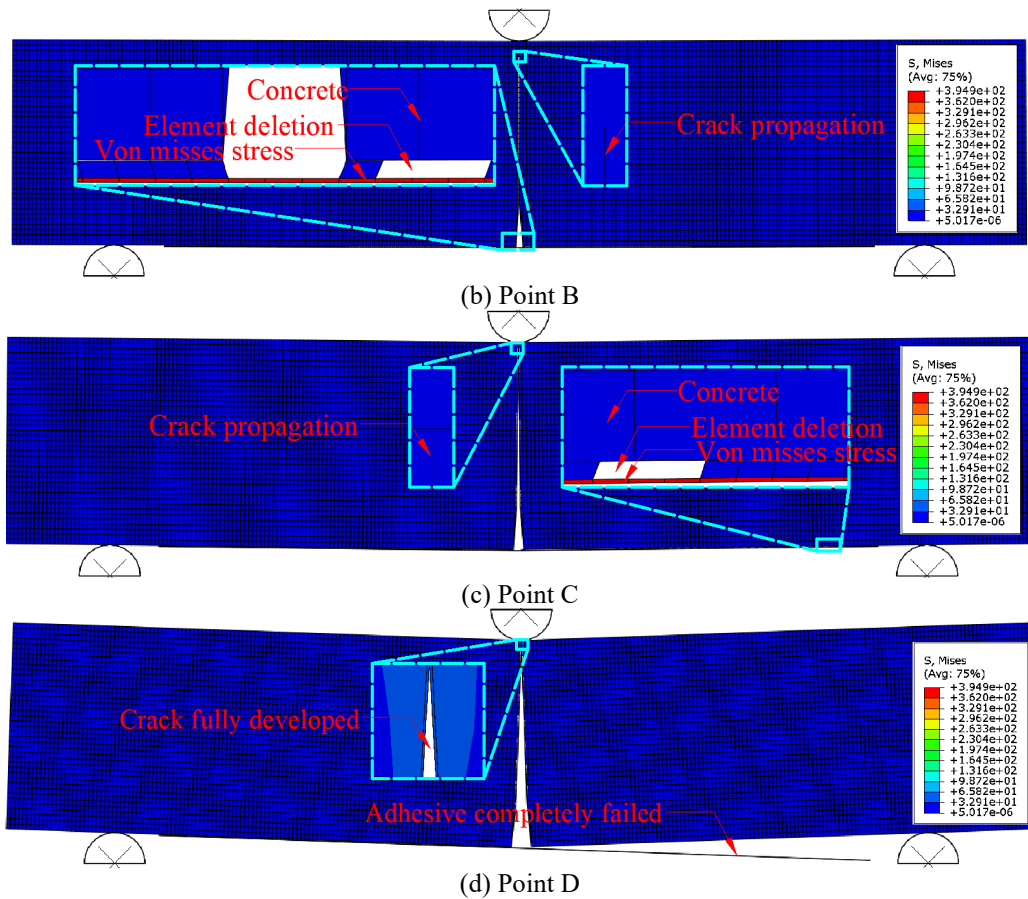


Fig. 10 - Schematic damage plot under delamination failure mode

5.2 Damage Plot under Shear Failure Mode

In shear failure mode, the crack was initiated from CFRP edge within concrete beam. As the concrete has reached maximum principle tensile stress, crack is exhibited within concrete beam. A typical load-displacement profile with shear failure mode is shown in Fig. 11 from notched concrete beam designation 20-100. Consequently, Fig. 12 depicted damage plot of each labelled key-points from load-displacement profile given in Fig. 11. Prior to point A, beam have not yet developed any crack and crack initiation is exhibited at point A. Crack is continues to propagate at approximately half beam depth to give ultimate load at failure at point B. Then, point C showed fully developed crack and concrete beam has completely lose its loading capacity. It can be seen that under shear failure, the crack propagates to under punch point which agrees to experimental observation reported in [8].

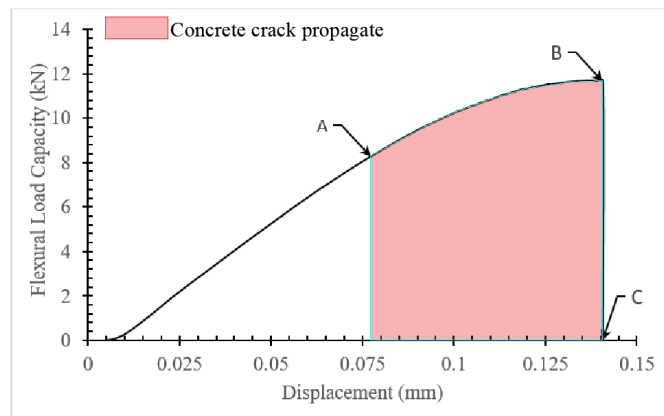


Fig. 11 - Load-displacement profile of concrete beam specimens failed in shear mode

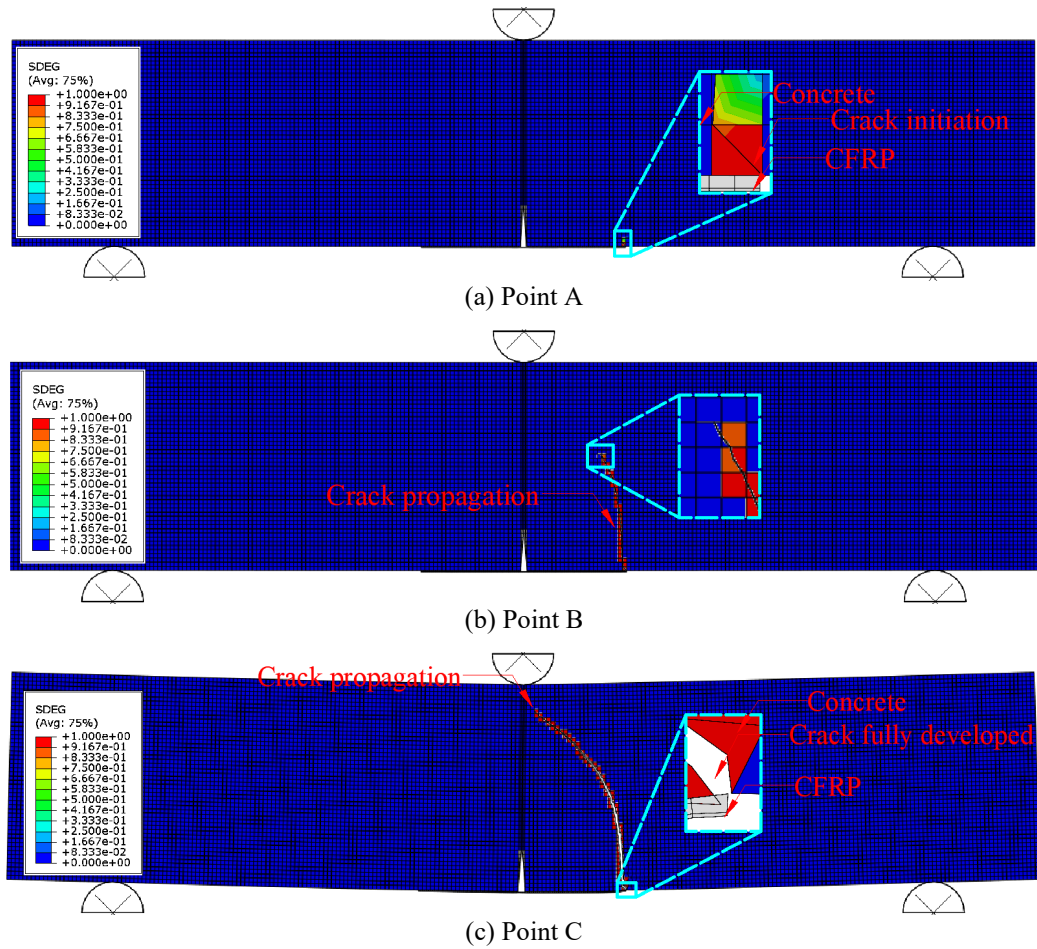
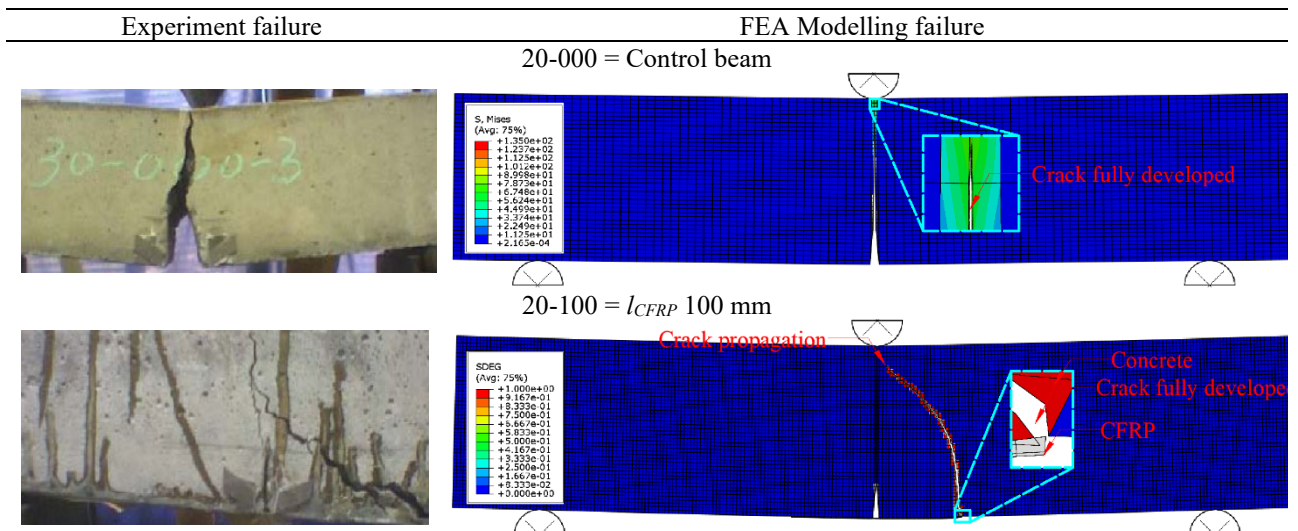


Fig. 12 - Schematic damage plot under shear failure mode

5.3 Damage Consistency with Experimental Investigation

Fig. 13 shows the comparison of experimental observation with FEA deformation of all concrete beams to consistence with failure modes and associated damage pattern. The initial flexural fracture was discovered to originate at the tension concrete face at the beam mid-span and followed by CFRP plate delamination (or CFRP debonding). On the contrary, shear failure demonstrated initial crack from CFRP plate edge as described in previous section. Experimental observations revealed that the shear failure mode was seen in notched beam with CFRP length of less than 200 mm and longer CFRP sheets (≥ 300 mm length) demonstrated delamination failures. Overall, the modelling graphical outputs of all tested concrete specimens showed good consistencies with reported experimental observations.



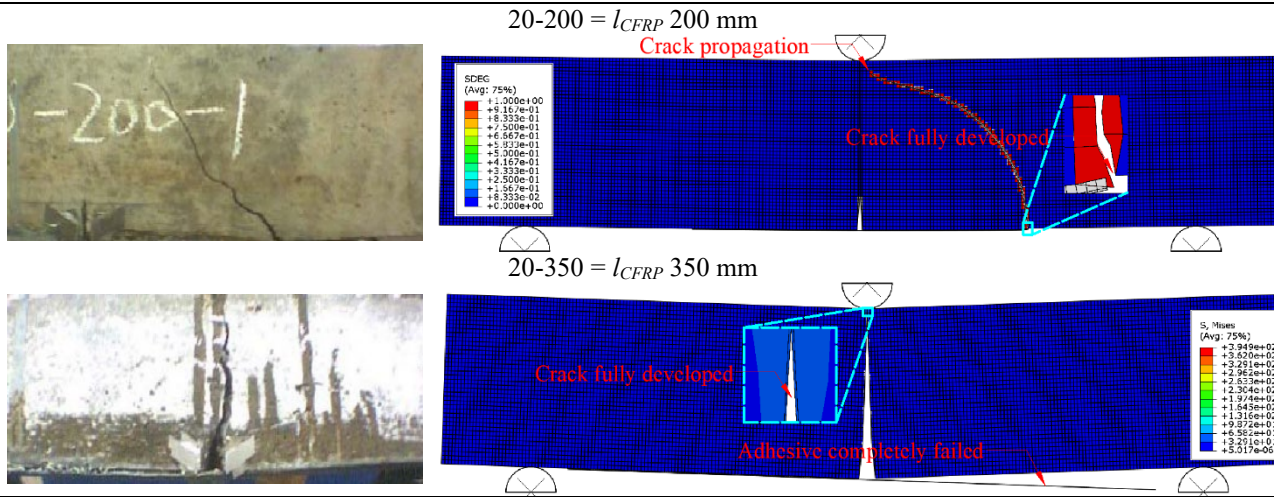


Fig. 13 - Damage consistency between FEA modelling and experimental observations in notched beam (after Ding et al. [22])

5.4 Validation with Experimental Output

As shown in Table 6 and Table 7, the experimental and numerical modelling discrepancy were in good agreements. Eq. (6) is the expression used to calculate the FEA modelling discrepancies. Bear in mind that the material properties utilized in traction separation relationship are not measured but it is calibrated from similar concrete grades and CFRP plates from other literatures (original authors has not measured fracture energy values but only unnotched (unstrengthened) strength of concrete beams are available). It is much expected that better prediction can be obtained if fracture energy values are independently measured from experimental works.

$$Error (\%) = \frac{|P_{max,exp} - P_{max,FEA}|}{P_{max,exp}} \times 100 \tag{6}$$

Table 6 - Load discrepancy between experimental and FEA Modelling for notched beam

Designation	Ultimate Load Experimental, $P_{ult,exp}$ (kN)	Ultimate Load FEA Modelling, $P_{ult,FEA}$ (kN)	Discrepancy (%)	Failure Modes
20-000	6.99	7.75	11%	Brittle fracture
20-100	11.69	11.69	0%	Shear failure
20-150	19.00	18.27	4%	Shear failure
20-200	19.28	22.13	15%	Shear failure
20-300	20.33	22.27	10%	Delamination
20-350	21.11	22.26	5%	Delamination

Table 7 - Load discrepancy between experimental and FEA Modelling for unnotched beam

Designation	Ultimate Load Experimental, P_{ult} (kN)	Ultimate Load FEA Modelling, P_{ult} (kN)	Discrepancy (%)	Failure Modes
G1-F0-0-N	18.47	17.09	7%	Brittle fracture
G1-F0-10-N	19.73	24.35	23%	Delamination
G1-F0-15-N	20.43	24.28	19%	Delamination
G1-F0-20-N	21.42	24.28	13%	Delamination
G1-F0-25-N	22.23	24.26	9%	Delamination

6. Conclusions

2D FEA models of externally-bonded FRP plates on concrete beams to explicitly incorporates surface interactions, frictional load transfer and beam deformations. Combination of XFEM and CZM techniques in conjunction with traction-separation law has been incorporated to model delamination and shear failure modes in strengthened concrete beam using

externally bonded CFRP sheets. Two benchmarking works were successfully developed and validated against experimental datasets and consistence with experimental observations. Sensitivity studies has been performed to assure the strength predictions are independent from mesh refinement and damage stabilization coefficients. From experimental datasets and FEA modelling output, the average discrepancy for notched beam and unnotched beam series are given as 7% and 14.5 % respectively, considered as in good agreements. Bear in mind that the fracture energy values used is calibrated from similar concrete grades and epoxy resin from other literatures. It is much expected that better strength prediction can be obtained if the fracture energy is independently measured from experimental set-up. Also, the applicability for similar testing models requires larger testing series to provide more unified approach.

Acknowledgement

This research was financially supported by Ministry of Higher Education Malaysia (MOHE) through Fundamental Research Grant Scheme (FRGS/1/2020/TK01/UTHM/02/4). We also want to thank Research Management Center (RMC), University Tun Hussein Onn Malaysia (UTHM) for sponsoring this work under Postgraduate Research Grant (GPPS) (Research Grant No. H685).

References

- [1] ACI 440.2R-02. (2002). Guide for the design and construction of externally bonded FRP Systems for strengthening concrete structures. American Concrete Institute.
- [2] Ye J., Yu J., Cui C., & Wang Y. (2021). Flexural size effect of ultra-high ductile concrete under different damage and ductility levels. *Cement and Concrete Composites*, 115(1), 1-12. <https://doi.org/10.1016/j.cemconcomp.2020.103852>
- [3] El-Sherif H. E., Wakjira T. G., & Ebead U. (2020). Flexural Strengthening of reinforced concrete beams using hybrid near-surface embedded/externally bonded fabric-reinforced cementitious matrix. *Construction and Building Materials*, 238(12), 1-12. <https://doi.org/10.1016/j.conbuildmat.2019.117748>.
- [4] Abdul N. H. K., Bhutta M. A. R., Jamaludin M. Y., Warid M. H., Ismail M., Rahman M. S., Yunus I., & Azman M. (2014). Kenaf fiber reinforced polymer composites for strengthening RC beams. *Journal of Advanced Concrete Technology*, 12(6), 167-177, 2014. doi:10.3151/jact.12.167.
- [5] Abed M. J., Fayyadh M. M., & Khaleel O. R. (2020). Effect of web opening diameter on performance and failure mode of CFRP repaired RC beams. *Materials Today: Proceedings*, Elsevier, 42(1), 388-398. <https://doi.org/10.1016/j.matpr.2020.09.591> 2214-7853/Ó.
- [6] Salama A. S. D., Hawileh R. A., & Abdalla J. A. (2019). Performance of externally strengthened RC beams with side-bonded CFRP sheets. *Composite Structures*, 212(6), 281-290. <https://doi.org/10.1016/j.compstruct.2019.01.045>.
- [7] Nguyen-Minh L., Vo-Le D., Tran-Thanh D., Pham T. M., Ho-Huu C., & Rovňák M. (2017). Shear capacity of unbonded post-tensioned concrete T-Beams strengthened with CFRP and GFRP U-wraps. *Composite Structures*, 184(7), 1011-1029. <http://dx.doi.org/10.1016/j.compstruct.2017.10.072>.
- [8] NCHRP-5495, 200. (2005). Simplified shear design of structural concrete members: Appendixes. Urbana. National Cooperative Highway Research Program. <https://doi.org/10.17226/22070>.
- [9] Huang X., Wang J., Zhang F. S. Niu S. & Ding J., (2014). An experimental investigation on the failure behavior of a notched concrete beam strengthened with carbon fiber-reinforced polymer. *International Journal of Polymer Science*, 2015(8), 1-17. <http://dx.doi.org/10.1155/2015/729320>.
- [10] CEB-FIB. (2001). Externally bonded FRP reinforcement for RC structures. *Comite Euro-International du Beton*.
- [11] Ali H., Assih J., & Li A. (2021). Flexural capacity of continuous reinforced concrete beams strengthened or repaired by CFRP/GFRP sheets. *International Journal of Adhesion and Adhesives*, 104(10), 1-12.
- [12] Mostofinejad D. & Moghaddas A. (2014). Bond efficiency of EBR and EBROG methods in different flexural failure mechanisms of FRP strengthened RC beams. *Construction and Building Materials*, 54(1), 605-614.
- [13] De Domenico D., Urso S., Borsellino C., Spinella N., & Recupero A. (2020). Bond behavior and ultimate capacity of notched concrete beams with externally-bonded FRP and PBO-FRCM systems under different environmental conditions. *Construction and Building Materials*, 265(10), 1-16.
- [14] Lee Y. S. & Ahmad H. (2019). XFEM modelling of single-lap kenaf fibre composite hybrid joints under quasi-static loading. *Plastics, Rubber and Composites*, 48(2), 48-56.
- [15] Nunes F. A. A., Campilho R. D. S. G., Cardoso M. G., & Silva F. J. G. (2019). Fracture envelope estimation of a structural adhesive by dedicated fracture tests. *Procedia Manufacturing*, 38(6), 1252-1259.
- [16] Orifici A. C. & Krueger R. (2012). Benchmark assessment of automated delamination propagation capabilities in finite element codes for static loading. *Finite Elements in Analysis and Design*, 54(10), pp.28-36.
- [17] Rarani M. & Sayedain M. (2019). Finite element modeling strategies for 2D and 3D delamination propagation in composite DCB specimens using VCCT, CZM and XFEM approaches. *Theoretical and Applied Fracture Mechanics*, 103(4), 1-10.

- [18] Tafazzolimoghaddam B. (2017). Computational mechanics of fracture and fatigue in composite laminates by means of XFEM and CZM. PhD Thesis, University of Sheffield.
- [19] Camanho P. P., Davila C. G. & Moura D. (2003). Numerical simulation of mixed-mode progressive delamination in composite materials damage and failure of non-conventional composite laminates view project. *Journal of Composite Materials*, 37(16), 1415-1438.
- [20] Karimi M. & Rouzegar J. (2021). A CA-XFEM for mixed-mode variable-amplitude fatigue crack growth. *Theoretical and Applied Fracture Mechanics*, 114(3), 1-12.
- [21] Zhang C., Cao P., Cao Y., & Li J. (2013). Using finite element software to simulation fracture behavior of three-point bending beam with initial crack. *Journal of Software*, 8(5), 1145-1150.
- [22] Ding, J, F. Wang, X. Huang, & S. Chen. (2014). The effect of CFRP Length on the failure mode of strengthened concrete beams. *Journal Polymers*, 6(7), 1705-1726.
- [23] Al-Rousan R. Z., Alhassan M. A., & AlShuqari E. A. (2018). Behavior of plain concrete beams with DSSF strengthened in flexure with anchored CFRP sheets - Effects of DSSF content on the bonding length of CFRP sheets. *Case Studies in Construction Materials*, 14(6), 1-22.
- [24] Mahmoud A. M. (2012). Strengthening of concrete beams having shear zone openings using orthotropic CFRP modeling. *Ain Shams Engineering Journal*, 3(3), 177-190.
- [25] Mohammadi T. & Wan B. (2013). Finite element modeling of debonding failure between FRP and Concrete undergoing mixed mode loading. *Proceeding of the Conference: FRPRCS-11*, Guimaraes, Portugal.
- [26] Darwin D., Barham S., Kozul R., & Luan S. (2021). Fracture energy of high-strength concrete. *ACI Materials Journal*, 98(5), 410-417.
- [27] Rodrigues M. F., Pedrosa B., Rebelo C., Blasón S., Muniz-calvente M. & Fernández-canteli A. C. (2017). Static and fatigue behaviour of Sikadur® -30 and Sikadur® -52 structural resin/adhesive. *Proceeding of the 2nd International Conference on Structural Integrity ICSI*, Madeira, Portugal.
- [28] Mahjoub R., Yatim J. M., Mohd Sam A. R. & Raftari M. (2014). Characteristics of continuous unidirectional kenaf fiber reinforced epoxy composites. *Materials and Design*, 64(9), 640-649.
- [29] Kasper Y., Albiez M., Ummenhofer T., Mayer C., Meier T., Choffat F., Ciupack Y., & Pasternak H. (2021). Application of toughened epoxy-adhesives for strengthening of fatigue-damaged steel structures. *Construction and Building Materials*, 275(2), 1-15.
- [30] Wang H. T. & Wu G. (2018). Bond-slip models for cfrp plates externally bonded to steel substrates. *Composite Structures*, 184(8), 1204-1214.
- [31] Munjiza A. & John N. W. M. (2001). Mesh size sensitivity of the combined FEM/DEM fracture and fragmentation algorithms. *Engineering Fracture Mechanics*, 69(2), 281-295.
- [32] Tijssens M. G. A., Sluys B. L. J. & Van G, E. (2000). Numerical simulation of quasi-brittle fracture using damaging cohesive surfaces. *European Journal of Mechanics, A/Solids*, 19(5), 761-779.
- [33] More S. T. & Bindu R. S. (2015). Effect of mesh size on finite element analysis of plate structure. *International Journal of Engineering Science and Innovative Technology*, 4(3), 181-185.
- [34] Koslan M. F. S., Zaidi A. M. A., Othman M. Z., Abdullah S., & Thanakodi S. (2013). The effect of mesh sizing toward deformation result in computational dynamic simulation for blast loading application. *Modern Applied Science*, 7(7), 23-28.